Chapter 4

Collimated proton beams from magnetized near-critical plasmas

---

Generation of collimated proton beams by linearly and circularly polarized lasers from magnetized near-critical plasmas has been investigated with the help of three dimensional (3D) particle-in-cell (PIC) simulations. Cyclotron effects induced by the presence of an axial magnetic field causes a reduction in the transverse momentum gained by the protons during the acceleration process. Moreover the hot electrons gyrate around the axial magnetic field which enhances the hot electron flow along the axial direction across the target rear side. This enhances the sheath field along the axial direction which can improve the collimation of the energetic proton beam. Protons accelerated by the linearly polarized laser are observed to have the highest collimation. However, protons accelerated by the right circularly polarized laser are not only highly collimated but are also more energetic as compared to the ones accelerated by the linearly polarized laser. Since, the proton transverse momentum has a significant contribution towards the total proton energy, the proton beams though become highly collimated but the maximum proton energy gets reduced in presence of an axial magnetic field.

4.1 Background of the study

Most of the ion acceleration experiments deal with solid target interactions. Near-critical plasmas such as cluster gas targets and foam targets can also be used to accelerate ions efficiently up to multi-MeV energies and also to enhance the collimation of energetic ion beam. Collimation is a very essential characteristic of accelerated ions which should be enhanced as the lack of collimation limits the use of high energetic ions for potential applications. Replenishable cluster targets facilitates high repetition rate of accelerated ions which are free from plasma debris and are highly collimated [1]. The motion of a laser pulse through near-critical plasma targets can lead to the formation of magnetic dipole structure which can accelerate the ions efficiently from the target rear side via magnetic vortex acceleration (MVA) [1–4] generating collimated energetic ions. Moreover, near-critical targets support the formation of plasma waveguide which makes it possible for the laser pulse to penetrate deeper into the plasma and generate abundant number of hot electrons. Nakamura et al. [5] have reported experimental results on ion acceleration from SiO_2 foam attached with a thin Al target. They have observed that the bulk electrons inside the foam region are heated up to MeV energies and abundant number of hot electrons are generated which increases the laser-plasma energy coupling and enhances the maximum ion energy. Bin et al. [6] have reported experimental results supported by three dimensional (3D) particle-in-cell (PIC) simulations on accelerating ions from carbon nanotube foams attached with thin diamondlike carbon targets. They have observed that the the high-intensity laser pulse on propagating through the near-critical carbon nanotube region undergoes relativistic self-focussing resulting in an extremely steep rising edge laser pulse profile which causes a significant enhancement in the carbon ion energies consistent with a transition to radiation pressure acceleration (RPA). Willingale et al. [7] have reported an experimental observation of a collimated He^{2+} ion beam generated via target normal sheath acceleration (TNSA) mechanism having a maximum energy of 40 MeV by a petawatt-class laser from a gas jet target. Ions can also be accelerated to multi-MeV energies from underdense plasmas [8]. A very high-intensity laser on propagation through the underdense plasma causes a ponderomotive expulsion of electrons from the high-intensity region at the central axis along the radial directions which creates a central ion channel. Thus, a large

space-charge field is generated which accelerates the ions along transverse directions via Coulomb explosion [9]. Ions can also be accelerated from underdense plasmas via collisionless shock acceleration [10]. However, these accelerated ions have poor collimation due to high transverse momentum. Willingale et al. [11] have reported experimental observations on the propagation of a high-intensity laser in foam targets generating energetic proton beams in the relativistic transparent regime. They have observed that the laser beam propagates deeper into the target due to its relativistic propagation and results in greater collimation of the hot electrons which enhances the rear surface accelerating field and hence increases the efficiency of acceleration.

Role played by the cyclotron effects induced by an axial magnetic field and the handedness of the polarization of a circularly polarized laser in accelerating protons from overdense plasmas has been discussed in detail in Chapter 3. However, these cyclotron effects can have a significant contribution in beam collimation in case of near-critical plasmas. Yang et al. [12] have shown that the plasma transparency in presence of magnetic field gets enhanced in case of a right circularly polarized (RCP) light which is beneficial for plasma acceleration. Wilson et al. [13] have presented an analytical description as well as 1D and 3D-PIC simulation results on the influence of externally applied strong magnetic fields on laser pulse propagation in an underdense plasma and have shown that the electron motion gets dramatically enhanced in case of a RCP light whereas in case of a left circularly polarized (LCP) light, the electron motion gets dampened and cause a reduction in instability growth.

In the present work, we investigate the role played by an axial magnetic field in accelerating protons and most importantly in enhancing the collimation of the accelerated protons from a near-critical plasma target by linearly polarized (LP) and circularly polarized (CP) laser pulses with the help of three dimensional (3D) particle-in-cell (PIC) simulations using the code Picpsi-3D [14]. It is observed that the collimation of proton beams increases significantly in presence of an axial magnetic field. Collimation is observed to be highest in case of a LP laser in presence of magnetic field. However, protons accelerated by a RCP laser are not only highly collimated but are also highly energetic having highest axial momentum.

4.2 3D-PIC Simulation Model

A laser propagating along Z direction of wavelength $\lambda = 1$ μm, normalized electric field amplitude $a_0(= eE_0/m_e\omega c) \approx 6$ which corresponds to an intensity of 5×10^{19} W/cm^2, pulse duration $\tau = 50$ fs (FWHM) is incident on a near-critical plasma target of density 3.35×10^{21} cm^{-3} (3 n_c). Here, $n_c = m_e\omega^2/4\pi e^2$ is the critical density where e and m_e are the charge and mass of an electron respectively, ω is the laser frequency, E_0 is the laser electric field amplitude and c is the speed of light. The spot size of the laser pulse is 3 μm (FWHM) and the laser period $T_0(= \lambda/c)$ is 3.3 fs. A simulation

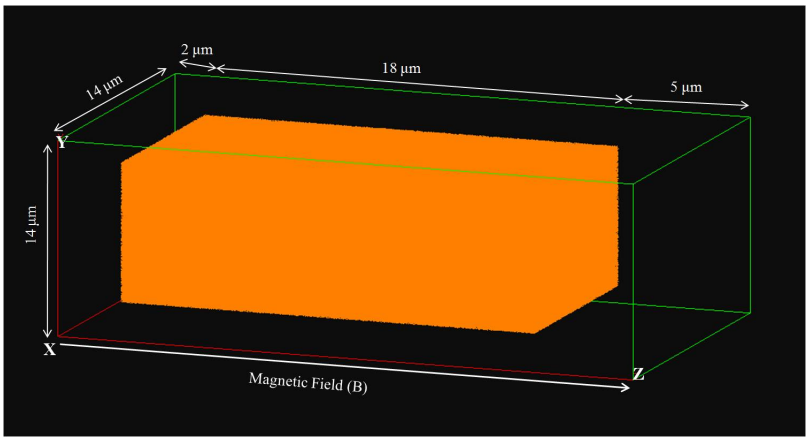

Fig. 4.1: 3D-PIC geometry of the simulation box.

box of dimensions 14 μm $\times$ 14 μm $\times$ 25 μm consisting of 140 $\times$ 140 $\times$ 250 cells has been used. The near-critical plasma of height and width 10 μm and thickness 18 μm is sharply edged and is located at a distance of 2 μm from the left boundary of the simulation box as shown in Fig. 1. The plasma thickness of 18 μm is chosen to ensure complete laser penetration. Since, the length $(= c\tau)$ of the laser pulse is 15 μm, the plasma thickness should be at least of the order of laser pulse length in order to achieve maximum penetration. This deep penetration results in volumetric heating of the plasma slab generating large number of hot electrons which can create strong electric fields. A magnetic field of B = 50 MG ($\omega_{ce}/\omega \approx 0.5$) is applied along Z which is the axial direction. The simulations have been done for five different cases (i) CP with B = 0 G, (ii) RCP with B = 50 MG, (iii) LCP with B = 50 MG, (iv) LP with B = 0 G and (v) LP with B = 50 MG. A vacuum gap of 5 μm is maintained across the target rear side in all cases. Absorbing boundary conditions has been incorporated along all the three directions. The simulations are done with 25 macroparticles per

cell. The ions considered in these simulations are protons with mass $m_i = 1836\ m_e$. $\omega_{pe} = \sqrt{4\pi n_e e^2/m_e}$ and $\omega_{ce} = eB/m_e c$ are the electron plasma frequency and electro cyclotron frequency respectively where n_e is the electron plasma density. The plasma is initially assumed to be cold with $T_e = T_i = 0$, where T_e and T_i are the electron and ion temperatures respectively.

4.3 Generation of collimated proton beams

The cyclotron effects play an important role in the generation of hot electrons. A RCP laser and a LCP laser act differently on electrons in presence of an axial magnetic field due to cyclotron effects. In case of a RCP laser, the direction of rotation of electrons by the laser electric field and the direction of electron gyrations by an axial magnetic field are same, which enhances the effect of the laser ponderomotive force. Hence, the electrons gain more energy in case of a RCP laser. On the other hand, in case of a LCP laser, the direction of electron rotations by the laser electric field and the axial magnetic field gyrations are opposite which reverses the cyclotron effects. This opposes the electron motion and causes a reduction in the electron energy. Thus, the electrons move longer distances on gaining higher energy in case of a RCP laser. Whereas, in case of a LCP laser, the electrons tend to get accumulated at the tip of the laser pulse, which may increase the local electron density at the laser pulse front [15].

The hot electrons reach the target rear side and forms a hot electron sheath which accelerates the protons from the target rear side via TNSA mechanism as shown in Fig. 4.2. Since, the electrons gain more energy by a RCP laser in presence of an axial magnetic field, the hot electrons reach the target rear side quickly and form the hot electron sheath. The axial sheath electric field is strongest in case of a RCP laser as compared to all the other cases at time 101 T_0 as shown in Fig. 4.2 (b2). Comparing Fig. 4.2 (b1) and 4.2 (b4), it can be observed that in absence of magnetic field, the sheath field by a CP laser is stronger than that by a LP laser. This might be due to the dominant effect of radiation pressure as the oscillatory component of the ponderomotive force is absent in case of a CP laser. Since, the transverse motion of the hot electrons generated by a LP laser gets restricted in presence of an axial

magnetic field, the hot electron number as well as the energy along the axial direction is increased which makes the sheath field stronger as shown in Fig. 4.2 (b5).

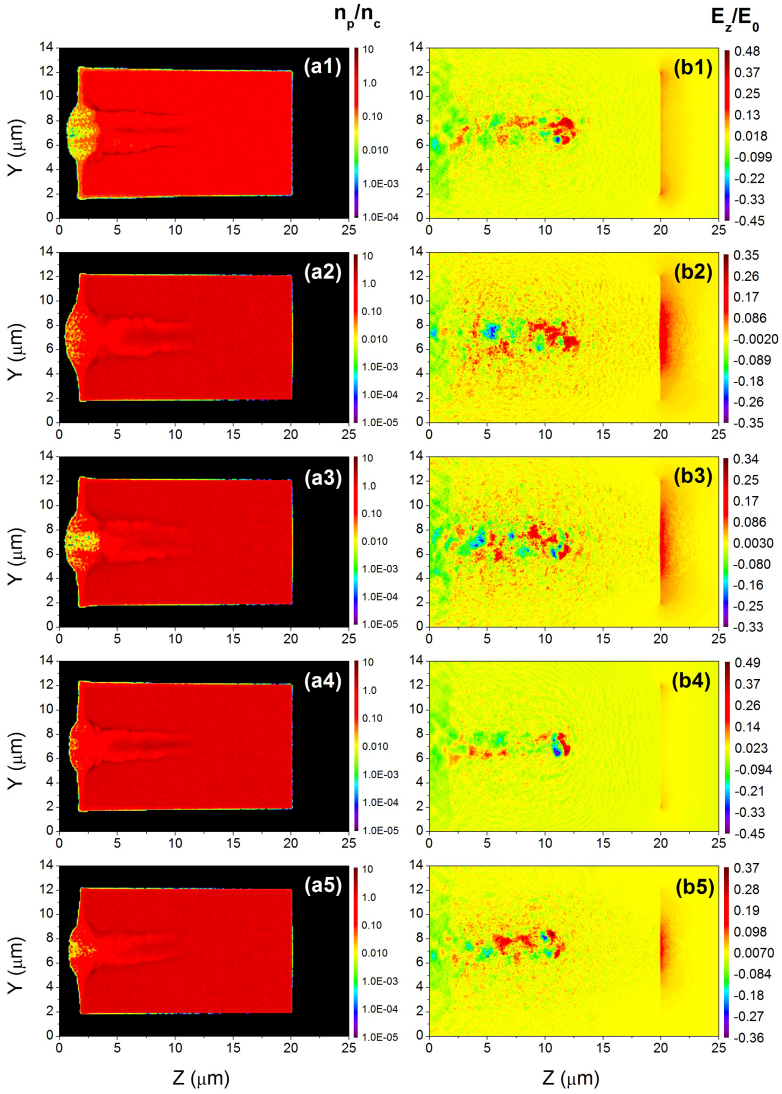

Fig. 4.2: Proton density distribution (a1-a5) and axial electric field (b1-b5) in the central YZ plane (X = 7 μm) at time 101 T_0 respectively for (a1,b1) CP with B = 0 G, (a2,b2) RCP with B = 50 MG, (a3,b3) LCP with B = 50 MG, (a4,b4) LP with B = 0 G and (a5,b5) LP with B = 50 MG. The proton density n_p is normalized by the critical density $n_c = 1.12 \times 10^{21}$ cm^{-3} and the axial electric field E_z is normalized by the laser electric field E_0.

Comparing all the five cases at time 101 T_0, it can be observed that the protons gain highest momentum at the target rear side in case of RCP laser in presence of an axial magnetic field due to efficient hot electron generation as shown in Fig. 4.3 (b). However, it can also be observed that the forward momentum gained by the protons at the target front side is higher in case of a CP laser in absence of magnetic field and LCP laser in presence of magnetic field as shown in Fig. 4.3 (a)

and (c) respectively. Since, the oscillatory component of the laser ponderomotive

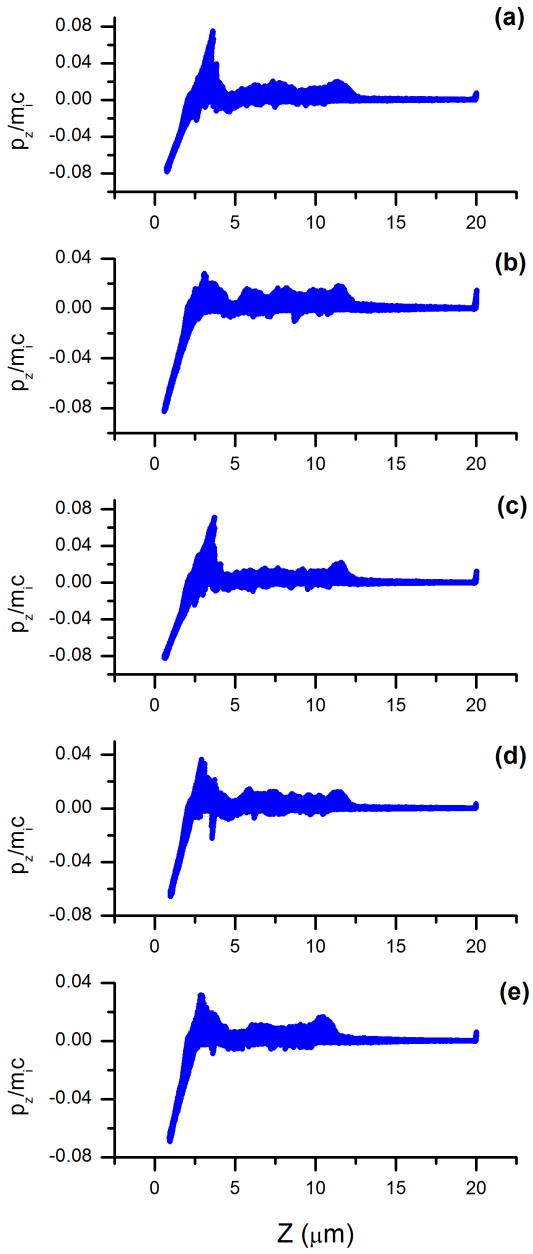

Fig. 4.3: Normalized proton axial momentum p_z/m_ic phase space for (a) CP with B = 0 G, (b) RCP with B = 50 MG, (c) LCP with B = 50 MG, (d) LP with B = 0 G and (e) LP with B = 50 MG at time 101 T_0.

force is absent in case of a CP laser, the radiation pressure can effectively form an electrostatic charge separation region at the target front side and accelerate protons in the forward direction. In case of a LCP laser, due to reverse cyclotron effects, there might be an electron accumulation at the laser pulse front which can strengthen the electrostatic charge separation region at the target front side and accelerate protons

effectively in the forward direction. Thus, traces of RPA accelerated protons are also

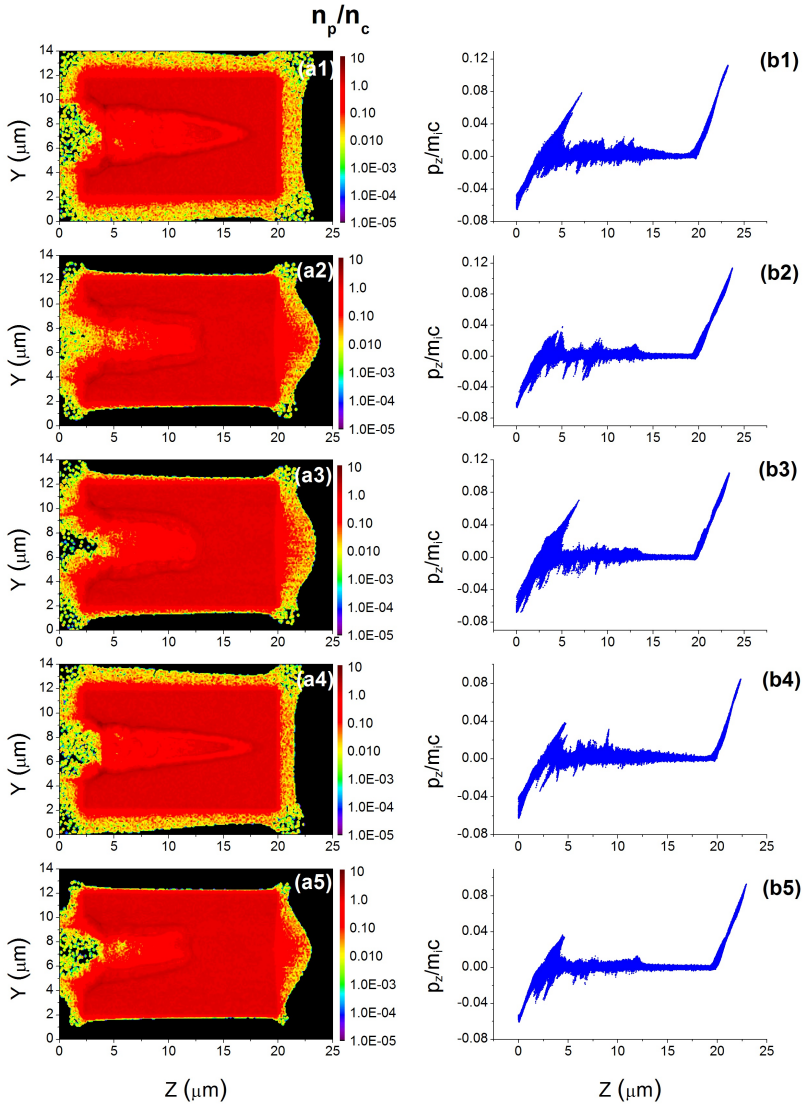

Fig. 4.4: Proton density distribution (a1-a5) in the central YZ plane (X = 7 μm) and normalized proton axial momentum p_z/m_ic phase space (b1-b5) at time 147 T_0 respectively for (a1,b1) CP with B = 0 G, (a2,b2) RCP with B = 50 MG, (a3,b3) LCP with B = 50 MG, (a4,b4) LP with B = 0 G and (a5,b5) LP with B = 50 MG. The proton density n_p is normalized by the critical density $n_c = 1.12 \times 10^{21}$ cm^{-3}.

observed in these two cases but TNSA overtakes the acceleration process eventually. Since, the ponderomotive force gets enhanced in case of a RCP laser, the electrons gain high energy and move fast across the target rear side which accelerate the protons via TNSA mechanism. Thus, front side acceleration is least and rear side acceleration is highest in case of a RCP laser in presence of an axial magnetic field. In case of a LP laser, the protons gain more momentum at the target rear side in presence of an axial magnetic field as the transverse hot electron motion is restricted

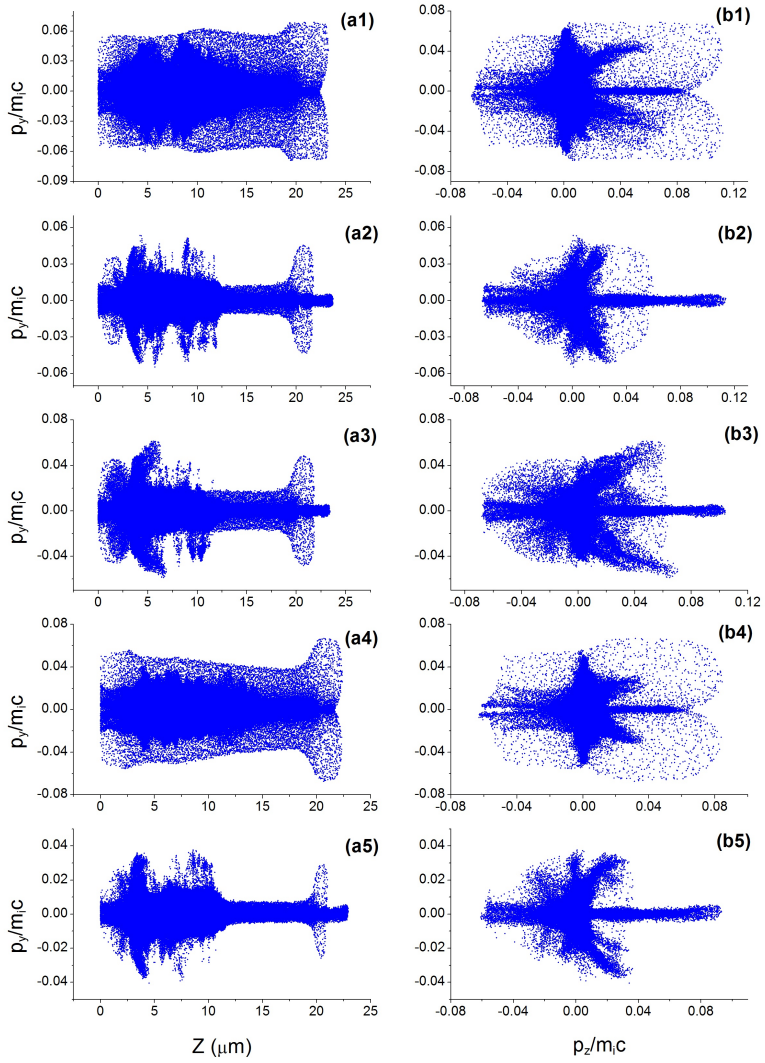

Fig. 4.5: Normalized proton momentum phase space (a1-a5) p_y/m_ic vs Z (μm) and (b1-b5) p_y/m_ic vs p_z/m_ic at time 147 T_0 respectively for (a1,b1) CP with B = 0 G, (a2,b2) RCP with B = 50 MG, (a3,b3) LCP with B = 50 MG, (a4,b4) LP with B = 0 G and (a5,b5) LP with B = 50 MG.

due to cyclotron effects resulting more number of hot electrons to flow along the axial direction and generate stronger sheath field which enhances the acceleration as shown in Fig. 4.3 (e).

The acceleration of protons at time 147 T_0 is shown in Fig. 4.4. The transverse motion of protons gets considerably reduced in presence of an axial magnetic field due to cyclotron effects as observed from the proton density plots shown in Fig. 4.4 (a1-a5). The protons gain highest forward momentum at the target rear side in case of a RCP laser as shown in Fig. 4.4 (b2). As evident from the proton axial momentum phase space plots, the protons are accelerated mainly via TNSA mechanism. It can

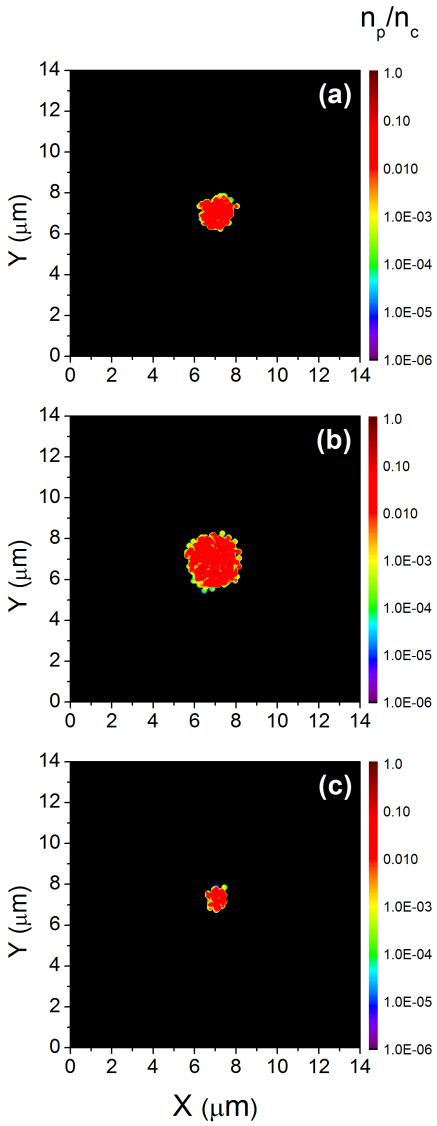

Fig. 4.6: Proton density distribution in the XY plane (Z = 23.6 μm) for (a) RCP with B = 50 MG at time 147 T_0, (b) LCP with B = 50 MG at time 150 T_0 and (c) LP with B = 50 MG at time 154 T_0. The proton density n_p is normalized by the critical density $n_c = 1.12 \times 10^{21}$ cm^{-3}.

also be observed from the proton density plots that the laser penetrates deeper into the plasma in the absence of magnetic field. Since, the plasma can expand freely in absence of magnetic field, the laser penetration doesn't get affected. The penetration decreases in presence of magnetic field due to restricted transverse electron motion which causes more number of hot electrons to be present along the axial direction. These hot electrons restrict laser pulse penetration.

A circularly polarized laser on propagation through an underdense plasma can generate an axial magnetic field via inverse Faraday effect (IFE) [16–20]. The direc-

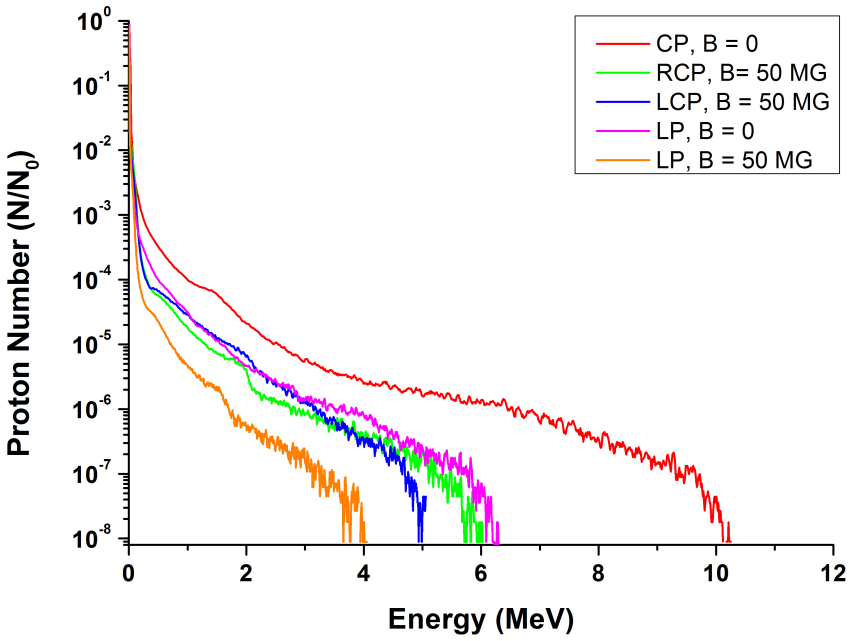

Fig. 4.7: Proton energy spectrum for CP with B = 0 G (red solid), RCP with B = 50 MG (green solid), LCP with B = 50 MG (blue solid), LP with B = 0 G (pink solid) and LP with B = 50 MG (orange solid) at time 147 T_0. The proton number N is normalized by the total number of protons N_0 in each case.

tion of such magnetic fields in case of a RCP and a LCP laser is opposite to each other [20]. These magnetic fields are localized within the laser pulse and do not penetrate in the surrounding plasma. The amplitude is highest along the laser axis and decreases along the transverse directions. These quasistationary magnetic fields are generated in a short time scale $\Delta t = r_0^2/c^2\tau$ [17] where r_0 is the radius of the laser pulse. For the present simulation parameters, we have $\Delta t \approx 0.5$ fs which is a very short time scale as compared to the acceleration time 147 T_0 which corresponds to ≈ 0.5 ps. Hence, the effect caused by these quasistatic short scale magnetic fields on the acceleration process would be negligible as compared to that caused by the static magnetic field. Moreover, unlike these quasistatic magnetic fields which exist only inside the laser pulse, the applied static magnetic field is present throughout the plasma which is essential for proper guiding of the hot electrons along the laser axis towards the target rear surface.

The axial and transverse momentum phase space plots for all the cases is shown in Fig. 4.5. It can be observed that the axial magnetic field significantly reduces the transverse momentum of the accelerated protons. The protons gain more momentum

along the laser axis in presence of an axial magnetic field which also causes an increase in the collimation of energetic protons. As the sheath electric field is built up at the target rear side and the protons start getting accelerated, they gain momentum both along the transverse and axial directions. This causes the transverse proton momentum to rise suddenly at the target rear side in all the cases which causes the formation of wing shaped patterns in the phase space as shown in Fig. 4.5 (a1-a5). Since, the transverse proton motion throughout the target is significantly reduced in presence of magnetic field, the transverse momentum seem to rise sharply at the target rear side in this case. This rise in transverse proton momentum experience a sharp fall making the wing shaped patterns more prominent and the protons emerge out as a highly collimated beam from the target rear side with remarkably reduced values of transverse momentum. Collimation of protons accelerated by a LP laser in presence of magnetic field appears to be highest due to smallest spot size among all the cases as shown in Fig. 4.6. However, the axial momentum is observed to be higher in case of a RCP laser as can be concluded by comparing Fig. 4.5 (b2) with 4.5 (b5). Moreover, the energy spectrum plotted in Fig. 4.7 shows that the protons accelerated by a LP laser though more collimated but are less energetic than those accelerated by a RCP laser in presence of magnetic field. In case of a LCP laser, the proton beams seem to be collimated but the number of protons having transverse momentum is also high as shown in Fig. 4.5 (b3). Hence, collimation in case of a LCP laser is not as effective as compared to that of a RCP laser. Moreover, the maximum proton energy obtained in case of a LCP laser is also lower than that of a RCP laser. Since, in absence of magnetic field the plasma doesn't experience any restriction in expansion along transverse directions, it becomes possible for the laser pulse to penetrate deeper and generate more number of energetic protons having higher values of transverse momentum. As the transverse motion of protons is restricted in presence of magnetic field, the number of protons having transverse momentum values is low. Since, the transverse momentum contributes significantly towards increasing the total energy of protons, the maximum proton energy is less in presence of magnetic field. The proton energy is thus observed to be highest in case of a CP laser in absence of magnetic field. The presence of magnetic field thus improves the beam collimation but in turn reduces the maximum energy.

In Chapter 3, the simulations were done for a comparatively dense target and it was observed that both RPA and TNSA were the actively participating mechanisms in the acceleration process. The axial magnetic field causes a synergy in these two processes which can be controlled by either using a RCP or a LCP laser. It was observed that RCP favours TNSA and LCP favours RPA. However, RPA was observed to be the dominating acceleration mechanism in case of dense targets. A minor enhancement of collimation was also observed. In the present work, since the plasma is near-critical, the laser is able to penetrate longer distance inside the plasma and TNSA is the dominating acceleration mechanism. Thus, the cyclotron effects are carried by the laser pulse itself deeper into the plasma which is responsible for the collimation. In case of a dense target, the cyclotron effects are carried on by the laser pulse up to the hole boring depth. Beyond this depth, the cyclotron effects are carried forward into the upstream region by the hot electrons generated at the target front surface. Hence, though a significant enhancement in the proton energy was observed but the collimation as speculated from the proton beam spot size was not significant as such.

Creation of a strong magnetic field of the order of 50 MG might seem to be difficult via conventional techniques. However, it is to be noted that the maximum proton energy in our simulations is obtained at a time ≈ 0.5 ps. Thus, instead of having a constant source of magnetic field, production of a high amplitude static magnetic field sustainable at least up to a time duration of ≈ 0.5 ps should serve the purpose of collimation as shown in our simulations.

4.4 Conclusion

The effect of an axial magnetic field on enhancing the collimation of the energetic proton beams generated from a near-critical plasma target has been investigated with the help of 3D-PIC simulations. The effect of laser pulse polarization combined with the cyclotron effects has also been studied by using both LP and CP laser pulses. The conclusions drawn from the above discussions can be summarized as follows:

i) Protons are observed to get accelerated via TNSA mechanism and the acceleration is higher in case of a CP laser than that of a LP laser.

ii) Presence of an axial magnetic field reduces the transverse motion of protons and enhances the axial momentum due to cyclotron effects.

iii) Traces of RPA protons are also observed in case of a CP laser in absence of magnetic field and LCP laser in presence of magnetic field. However, TNSA appears to be enhanced in case of a RCP laser in presence of magnetic field.

iv) In case of a LP laser, the presence of an axial magnetic field increases the acceleration as the transverse hot electron motion is reduced due to cyclotron effects and the hot electron flow across the rear side along the axis is increased resulting stronger sheath formation and hence enhanced acceleration.

v) Presence of an axial magnetic field significantly enhances the collimation of proton beams. Collimation appears to be highest in case of a LP laser in presence of magnetic field due to its smallest spot size. However, proton axial momentum is observed to be highest with good collimation in case of a RCP laser in presence of magnetic field.

vi) When the acceleration process starts, transverse proton momentum rises sharply at the target rear side. In presence of magnetic field, the transverse momentum after rising falls sharply due to cyclotron effects and the proton beams emerge out into the vacuum with very low values of transverse momentum and are therefore highly collimated.

vii) It is observed that though presence of magnetic field enhances collimation but in turn reduces maximum proton energy. This might be due to reduction in transverse momentum which has a significant contribution in the total proton energy.

Bibliography

[1] Fukuda, Y., Faenov, A. Y., Tampo, M., Pikuz, T. A., Nakamura, T., Kando, M., Hayashi, Y., Yogo, A., Sakaki, H., Kameshima, T., Pirozhkov, A. S., Ogura, K., Mori, M., Esirkepov, T. Z., Koga, J., Boldarev, A. S., Gasilov, V. A., Magunov, A. I., Yamauchi, T., Kodama, R., Bolton, P. R., Kato, Y., Tajima, T., Daido, H., and Bulanov, S. V. Energy increase in multi-mev ion acceleration in the interaction of a short pulse laser with a cluster-gas target. *Phys. Rev. Lett.*, 103: 165002, 2009.

[2] Bulanov, S. V. and Esirkepov, T. Z. Comment on "collimated multi-mev ion beams from high-intensity laser interactions with underdense plasma". *Phys. Rev. Lett.*, 98:049503, 2007.

[3] Bulanov, S. S., Bychenkov, V. Y., Chvykov, V., Kalinchenko, G., Litzenberg, D. W., Matsuoka, T., Thomas, A. G. R., Willingale, L., Yanovsky, V., Krushelnick, K., and Maksimchuk, A. Generation of gev protons from 1 pw laser interaction with near critical density targets. *Physics of Plasmas*, 17(4):043105, 2010.

[4] Nakamura, T., Bulanov, S. V., Esirkepov, T. Z., and Kando, M. High-energy ions from near-critical density plasmas via magnetic vortex acceleration. *Phys. Rev. Lett.*, 105:135002, 2010.

[5] Nakamura, T., Tampo, M., Kodama, R., Bulanov, S. V., and Kando, M. Interaction of high contrast laser pulse with foam-attached target. *Physics of Plasmas*, 17(11):113107, 2010.

[6] Bin, J. H., Ma, W. J., Wang, H. Y., Streeter, M. J. V., Kreuzer, C., Kiefer, D., Yeung, M., Cousens, S., Foster, P. S., Dromey, B., Yan, X. Q., Ramis, R., Meyer-ter Vehn, J., Zepf, M., and Schreiber, J. Ion acceleration using relativistic pulse shaping in near-critical-density plasmas. *Phys. Rev. Lett.*, 115:064801, 2015.

[7] Willingale, L., Mangles, S. P. D., Nilson, P. M., Clarke, R. J., Dangor, A. E., Kaluza, M. C., Karsch, S., Lancaster, K. L., Mori, W. B., Najmudin, Z., Schreiber, J., Thomas, A. G. R., Wei, M. S., and Krushelnick, K. Collimated

multi-mev ion beams from high-intensity laser interactions with underdense plasma. *Phys. Rev. Lett.*, 96:245002, 2006.

[8] Krushelnick, K., Clark, E. L., Najmudin, Z., Salvati, M., Santala, M. I. K., Tatarakis, M., Dangor, A. E., Malka, V., Neely, D., Allott, R., and Danson, C. Multi-mev ion production from high-intensity laser interactions with underdense plasmas. *Phys. Rev. Lett.*, 83:737–740, 1999.

[9] Sarkisov, G. S., Bychenkov, V. Y., Novikov, V. N., Tikhonchuk, V. T., Maksimchuk, A., Chen, S.-Y., Wagner, R., Mourou, G., and Umstadter, D. Self-focusing, channel formation, and high-energy ion generation in interaction of an intense short laser pulse with a he jet. *Phys. Rev. E*, 59:7042–7054, 1999.

[10] Wei, M. S., Mangles, S. P. D., Najmudin, Z., Walton, B., Gopal, A., Tatarakis, M., Dangor, A. E., Clark, E. L., Evans, R. G., Fritzler, S., Clarke, R. J., Hernandez-Gomez, C., Neely, D., Mori, W., Tzoufras, M., and Krushelnick, K. Ion acceleration by collisionless shocks in high-intensity-laser˘underdense-plasma interaction. *Phys. Rev. Lett.*, 93:155003, 2004.

[11] Willingale, L., Nagel, S. R., Thomas, A. G. R., Bellei, C., Clarke, R. J., Dangor, A. E., Heathcote, R., Kaluza, M. C., Kamperidis, C., Kneip, S., Krushelnick, K., Lopes, N., Mangles, S. P. D., Nazarov, W., Nilson, P. M., and Najmudin, Z. Characterization of high-intensity laser propagation in the relativistic transparent regime through measurements of energetic proton beams. *Phys. Rev. Lett.*, 102:125002, 2009.

[12] Yang, X. H., Yu, W., Xu, H., Yu, M. Y., Ge, Z. Y., Xu, B. B., Zhuo, H. B., Ma, Y. Y., Shao, F. Q., and Borghesi, M. Propagation of intense laser pulses in strongly magnetized plasmas. *Applied Physics Letters*, 106(22):224103, 2015.

[13] Wilson, T. C., Li, F. Y., Weikum, M., and Sheng, Z. M. Influence of strong magnetic fields on laser pulse propagation in underdense plasma. *Plasma Physics and Controlled Fusion*, 59(6):065002, 2017.

[14] Upadhyay, A., Patel, K., Rao, B. S., Naik, P. A., and Gupta, P. D. Three-dimensional simulation of laser–plasma-based electron acceleration. *Pramana*, 78(4):613–623, 2012.

[15] Kuri, D. K., Das, N., and Patel, K. Proton acceleration from magnetized overdense plasmas. *Physics of Plasmas*, 24(1):013112, 2017.

[16] Steiger, A. D. and Woods, C. H. Intensity-dependent propagation characteristics of circularly polarized high-power laser radiation in a dense electron plasma. *Phys. Rev. A*, 5:1467–1474, 1972.

[17] Bychenkov, V. Y. and Tikhonchuk, V. Magnetic field generation by short ultraintense laser pulse in underdense plasmas. *Laser and Particle Beams*, 14(1): 5562, 1996.

[18] Berezhiani, V. I., Mahajan, S. M., and Shatashvili, N. L. Theory of magnetic field generation by relativistically strong laser radiation. *Phys. Rev. E*, 55:995–1001, 1997.

[19] Gorbunov, L. M. and Ramazashvili, R. R. Magnetic field generated in a plasma by a short, circularly polarized laser pulse. *Journal of Experimental and Theoretical Physics*, 87(3):461–467, 1998.

[20] Naseri, N., Bychenkov, V. Y., and Rozmus, W. Axial magnetic field generation by intense circularly polarized laser pulses in underdense plasmas. *Physics of Plasmas*, 17(8):083109, 2010.